Refereed Proceedings

The 12th International Conference on Fluidization - New Horizons in Fluidization Engineering

Engineering Conferences International *Year* 2007

A New Fluid Dynamic Model for the CFD Simulations of Fluidized Beds

Luca Mazzei* Paola Lettieri†

*University College London, l.mazzei@ucl.ac.uk

†University College London, p.lettieri@ucl.ac.uk

A NEW FLUID DYNAMIC MODEL FOR THE CFD SIMULATIONS OF FLUIDIZED BEDS

Luca Mazzei, Paola Lettieri

Department of Chemical Engineering, University College London, Torrington Place,

London WC1E 7JE, UK

l.mazzei@ucl.ac.uk , p.lettieri@ucl.ac.uk

ABSTRACT

A new Eulerian-Eulerian multidimensional model is proposed for the study of the dynamics of dense fluidized suspensions. The main distinctive feature of this new formulation of the equations of motion resides in the closure relationships adopted to express the fluid-particle interaction force. The force accounts for three contributions: buoyant force, drag force and elastic force. The buoyant force is related to the weight of the fluid displaced by the particles. The drag force is expressed as the product of the drag exerted on an unhindered particle, subject to the same volumetric flux of fluid, and a “corrective function” dependent on both bed voidage and particle Reynolds number. The elastic force is related to spatial gradients in the bed voidage and is parallel to the drag force; the force can be regarded as the component of the drag which arises when the homogeneity of the suspension is lost at the macroscopic length scale. The model is used to study the fluidization dynamics of liquid-solid homogeneous beds and gas-solid bubbling beds with particles belonging to the Group B of the Geldart's classification (1). The results of the simulations are compared with experimental data mainly in terms of average bed height, average bed voidage and diameter of the rising bubbles.

INTRODUCTION

Since its very first commercial applications, the technique of fluidization has attracted more and more the attention of the industrial world, which didn't fail to recognize and appreciate the potential offered by this innovative technology.

Albeit used extensively in commercial operations, nonetheless fluidization still poses a major challenge to engineers when tackling the design of new industrial plants. These, for their very nature, are highly dependent on their hydrodynamic behavior which in turn is affected by the system geometry and size. Critical scale-up problems therefore arise, related to how accurately changes in performance with plant size can be accounted for at the design stage.

In this regard, CFD has proved a valuable research means; the aim is succeeding in simulating and investigating the behavior of full-size units, so as to add insight into the passage from pilot plants to industrial ones, and render the latter less uncertain

The 12th International Conference on Fluidization - New Horizons in Fluidization Engineering, Art. 84 [2007]

and risky. To this purpose, it is nevertheless critical that accurate models be developed, along with appropriate constitutive equations. This work proposes a new Eulerian-Eulerian multidimensional model for the analysis of the fluid dynamic behavior of dense fluidized suspensions.

EQUATIONS OF CHANGE

The general formulation of the Eulerian-Eulerian locally averaged equations of change for dense fluidized suspensions is reported hereunder. For the fluid phase, in the assumption that the fluid is incompressible, the conservation of mass (continuity equation) and linear momentum yield:

$$\frac{\partial \varepsilon}{\partial t} + \vec{\nabla} \cdot \left(\varepsilon \, \vec{u}_f \right) = 0 \tag{1}$$

$$\rho_f \frac{\partial}{\partial t}\left(\varepsilon \, \vec{u}_f \right) + \rho_f \vec{\nabla} \cdot \left(\varepsilon \, \vec{u}_f \vec{u}_f \right) = \vec{\nabla} \cdot \overline{\overline{T}}_f - n_p \, \vec{\Phi}_{fp} + \varepsilon \, \rho_f \, \vec{g} \tag{2}$$

Similarly, for the solid phase, we have:

$$\frac{\partial \phi}{\partial t} + \vec{\nabla} \cdot \left(\phi \, \vec{u}_p \right) = 0 \tag{3}$$

$$\rho_p \frac{\partial}{\partial t}\left(\phi \, \vec{u}_p \right) + \rho_p \vec{\nabla} \cdot \left(\phi \, \vec{u}_p \vec{u}_p \right) = \vec{\nabla} \cdot \overline{\overline{T}}_p + n_p \, \vec{\Phi}_{fp} + \phi \, \rho_p \, \vec{g} \tag{4}$$

Here ε and ϕ, ρ_f and ρ_p, and $\vec{u}_f$ and $\vec{u}_p$ are the volume fractions, densities and velocities of fluid phase and solid phase respectively. n_p is the particle number density, and $\vec{g}$ is the gravitational acceleration. $\overline{\overline{T}}_f$ and $\overline{\overline{T}}_p$ represent the fluid and the solid stress tensors, and $\vec{\Phi}_{fp}$ denotes the interaction force per unit particle exerted by the fluid phase on the solid phase. Note that the sum of the fluid and solid volume fractions always equals one: $\varepsilon + \phi = 1$.

CLOSURE RELATIONSHIPS

The Eulerian-Eulerian locally averaged equations of change for a fluidized suspension of solid particles take always the form reported in the previous section. Thus, the feature of each specific model is not to be found in the formulation of such equations, but lies in the constitutive expressions used to close the terms $\overline{\overline{T}}_f$, $\overline{\overline{T}}_p$ and $\vec{\Phi}_{fp}$.

Stress tensor closures

The constitutive equation used to express the stress tensor of the fluid phase is that usually employed for compressible Newtonian fluids:

$$\overline{\overline{T}}_f = -\vec{\nabla} p + \mu_f \left[\vec{\nabla} \vec{u}_f + \left(\vec{\nabla} \vec{u}_f \right)^T - \frac{2}{3} \left(\vec{\nabla} \cdot \vec{u}_f \right) \overline{\overline{I}} \right] \tag{5}$$

where p and μ_f are the fluid pressure and viscosity respectively, and $\bar{\bar{I}}$ is the identity tensor.

In this analysis, the contribution due to the solid stress tensor is neglected. This choice is made intentionally. Indeed, this work is part of an ongoing study which proposes, among other things, to compare the results derived from the present formulation of the model with those obtained by including in the solid phase dynamical equation the contribution due to the solid stress tensor. In this regard, it should be emphasized that the inclusion of such term is not irreconcilable with the modeling choices herein undertaken and, in particular, with the concept of elastic force. Whereas such force is fluid dynamical in nature and is part of the fluid-particle interaction *between* the phases, the solid stress is related to the interactions between the particles *within* the solid phase and is totally unrelated to the fluid presence.

Interaction force closures

The fluid-particle interaction force is modeled as the sum of three contributions, namely: buoyant force, drag force and elastic force. We can write:

$$n_p \vec{\Phi}_{fp} = n_p \vec{f}_s + n_p \vec{f}_k + n_p \vec{f}_e \tag{6}$$

Before going any further, it is worth pointing out that other contributions to the fluid-particle interaction force should in general be considered; we mention, for instance, the virtual mass force, the lift force and the fluid local acceleration force. Especially the latter, at least from a theoretical point of view, plays sometimes an important role (2). In the present study, however, since such contributions are not dominant, they have been neglected.

The buoyant force is expressed using the “classical" definition of buoyancy which regards the force as equal to the weight of the fluid displaced by the particles:

$$n_p \vec{f}_s = -\phi \rho_f \vec{g} \tag{7}$$

This definition differs substantially from those employed in most multiphase flow models where the force is usually assumed to be proportional either to the fluid pressure gradient or to the divergence of the fluid stress tensor:

$$n_p \vec{f}_s^{\,*} = -\phi \vec{\nabla} p \quad ; \quad n_p \vec{f}_s^{\,**} = -\phi \vec{\nabla} \cdot \bar{\bar{T}}_f \tag{8}$$

Here the classical definition of buoyant force, equation (7), is preferred; this, as opposed to equation (8), preserves the distinctive feature of such force: its being *constant* and altogether unrelated to the specific characteristics of the flow field (3).

The drag force closure that we propose is the following:

$$n_p \vec{f}_k = \beta \left(\vec{u}_f - \vec{u}_p \right) \tag{9}$$

The 12th International Conference on Fluidization - New Horizons in Fluidization Engineering, Art. 84 [2007]

where the function β is given by the constitutive expression:

$$\beta = \frac{3}{4} C_D(\mathrm{Re}) \frac{\rho_f \left| \vec{u}_f - \vec{u}_p \right| (1-\varepsilon)}{d_p} \varepsilon^{-\psi(\varepsilon,\mathrm{Re})} \qquad (10)$$

Here $C_D(\mathrm{Re})$ is the drag coefficient and d_p is the particle diameter. $\psi(\varepsilon,\mathrm{Re})$ is a "corrective function" dependent on both particle Reynolds number and bed voidage. This dependence is not found in the majority of multiphase flow models where the exponent is usually assumed to be constant and equal to 2.65, 2.70 or 2.80. It is not possible here to provide the analytical expression for $\psi(\varepsilon,\mathrm{Re})$ due to the page constraint imposed for the article. We have chosen, therefore, to report $\psi(\varepsilon,\mathrm{Re})$ in the form of a diagram, referring for more details to the work by Mazzei et al. (4). In Figure 1a theoretical values of $\psi(\varepsilon,\mathrm{Re})$ are compared with empirical ones obtained from experimental data published in literature by Happel and Epstein (5) and Rumpf and Gupte (6) with regard to homogeneous assemblies of mono-sized particles fluidized by means of liquids. This diagram confirms the variability of the exponent with the particle Reynolds number and the bed void fraction. Figure 1b, similarly, compares theoretical values of $\psi(\varepsilon,\mathrm{Re})$ to experimental ones (still obtained from empirical data published by several groups of researchers) and emphasizes once again the variability of the exponent. In the figure also other closures are considered, more specifically that developed by Wen and Yu (7) and that based on the empirical correlation by Ergun (8) originally developed for the assessment of the unrecoverable pressure drop through packed beds (for this last drag force closure, since no exponential corrective function is present, an equivalent exponent is worked out). As we note, the experimental exponent varies in the range 1.9 - 2.9 and is by no means constant.

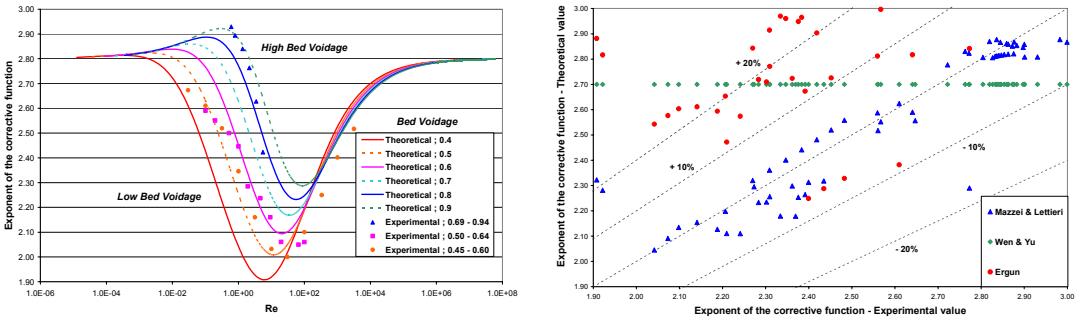

Figure 1: Comparison between theoretical and experimental values of $\psi(\varepsilon,\mathrm{Re})$.

The elastic force closure is the following:

$$n_p \vec{f}_e = -\frac{2}{3} d_p \left(\vec{\nabla}\varepsilon \cdot \vec{n}_k \right) \zeta(\varepsilon,\mathrm{Re}) \, n_p \vec{f}_k \qquad (11)$$

where $\vec{n}_k$ is the drag force unit vector, and $\zeta(\varepsilon,\mathrm{Re})$ is a constitutive scalar function dependent on the particle Reynolds number and fluid volume fraction. For more details regarding equation (11) we refer to the work by Mazzei et al. (4).

Homogeneous fluidized beds

The fluidization dynamics of a Geldart Group A powder (mean particle diameter: 253 μm, solid density: 2780 kg/m^3) fluidized by water (ambient operating conditions) is simulated using the model just presented. The purpose of the study is to investigate the dynamics of homogeneous beds and to test computationally the validity of the drag force closure advanced by the present authors. From these simulations, however, no information can be elicited as regards the elastic force, since in homogeneous systems such force is absent as no gradients in the bed voidage are present. Each simulation starts considering a fixed bed with voidage equal to 0.4. At time t=0 water is fed; four different values for the superficial velocity are used: 0.272 cm/s, 0.528 cm/s, 0.925 cm/s and 1.50 cm/s. Three different drag force closures are employed: the new constitutive relationship presented in this paper, the closure suggested by Wen and Yu (7), and the equation based on the empirical correlation developed by Ergun (8). The equations of motion are solved in each case using the commercial CFD code CFX 4.4; the integration is performed using a time step of 0.01 seconds. The computational results are compared to experimental data obtained, for the same system, by Richardson and Zaki (9).

Figure 2a presents the results in terms of bed voidage. As we can see, the new constitutive equation herein advanced proves very accurate and improves the predictions in terms of bed expansion. This provides an indirect proof of a better assessment of the drag force magnitude. Figure 2b reports the percent error as a function of the bed voidage. This figure confirms the better predictive capability of the new drag force closure.

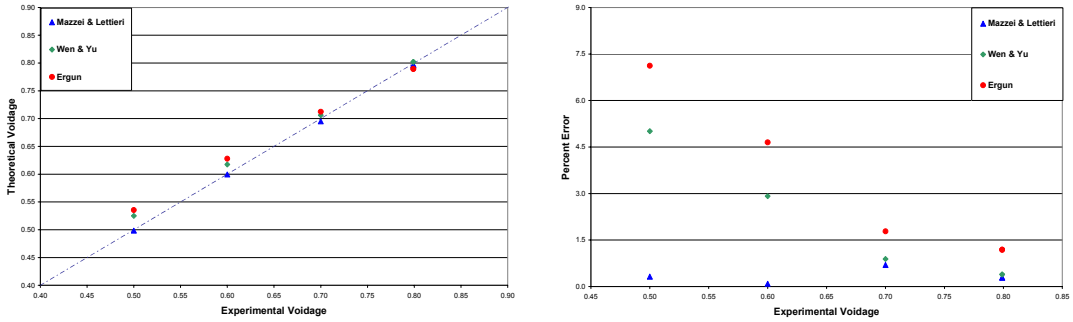

Figure 2a & 2b: Comparison between theoretical and experimental values of the bed voidage and percent error of the computational results obtained using alternative drag force closures.

It is interesting to note that the constitutive equation based on the Ergun correlation improves in accuracy with increasing values of the bed voidage. This might seem somewhat surprising if we think that the original correlation on which the closure is based catered solely for fixed beds. The explanation for this apparent inconsistency is simple: it can be shown that in the intermediate regime (that is, the fluid dynamic region between the purely viscous and the purely inertial regimes) the Ergun closure is better predictive at high bed void fractions and not at low ones as it might be expected. In this regard, we refer to Figure 3. Here we report the ratio between the equilibrium void fraction in homogeneous liquid-fluidized beds obtained from a) the

The 12th International Conference on Fluidization - New Horizons in Fluidization Engineering, Art. 84 [2007]

linear momentum balance solved using the Ergun drag force closure, and b) the Richardson and Zaki empirical correlation. The ratio is reported as a function of the Reynolds number parameterized in the experimental voidage. A perfect fit is obtained when the ratio is equal to one. The diagram clearly shows that in the intermediate fluid dynamic region the accuracy of the Ergun drag force closure improves with increasing bed void fractions. This provides a clear explanation of the seemingly contradictory numerical results.

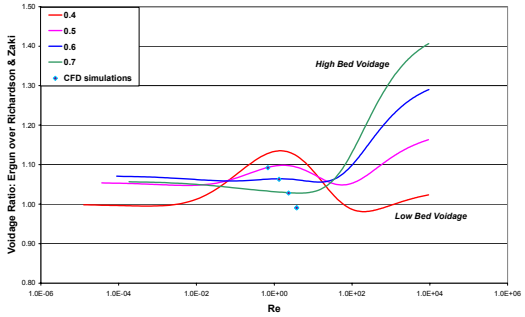

Figure 3: Ratio between the equilibrium void fraction in homogeneous liquid-fluidized beds obtained from a) the linear momentum balance solved using the Ergun drag force closure, and b) the Richardson and Zaki empirical correlation.

Bubbling fluidized beds

The fluidization dynamics of a Geldart Group B powder (diameter: 350 μm, density: 2500 kg/m^3) fluidized by air (ambient operating conditions) is also simulated using the multiphase model herein advanced. The initial conditions are the same as those employed in the previous study. The superficial velocity is fixed at 0.25 m/s. The mathematical model is solved using the commercial CFD code CFX 4.4. Figure 4 reports the results of the simulation (for the first three seconds) expressed in terms of bed voidage profile.

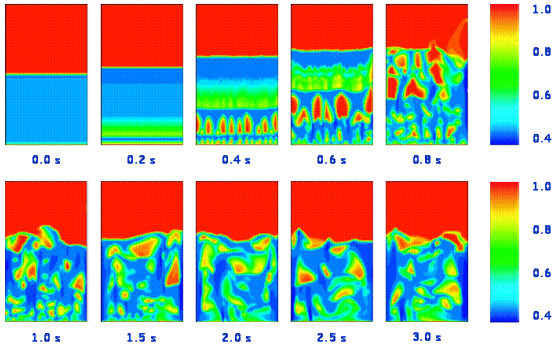

Figure 4: Voidage profile as a function of time.

The results shown in Figure 4 are just qualitative since the simulation is still not finished at the time of writing. Once the end of the simulation is reached, the results will be validated by comparing them with experimental data. More specifically, the validation will be performed in terms of average voidage of the bed, bed height, pressure drop through the bed, bubbles diameters and shapes and bubbles rise velocities. To work out the equivalent diameter of the bubbles from the output data provided by the CFD simulations, a numerical algorithm has been implemented by

Mazzei and Lettieri (10). This, using the computed voidage profile, generates a computational grid made up of zeros and ones (zero indicating absence of solid, one indicating presence of solid) where the geometrical properties of the bubbles are captured and can be assessed quantitatively without any task to be performed by the CFD user. The grid generated by the algorithm is therefore a mere working tool used by the program in order to carry out the computations automatically and rapidly. An example of such grid is reported in Figure 5a; this has been generated by the algorithm and refers to the bottom part of the bed as it appears after 0.6 seconds from the beginning of the simulation. The shape of the bubbles featuring in Figure 5a and Figure 5b can be compared; as we can see the bubble shapes are not altered and the grid captures all the significant geometrical properties of the bubbles. It is worth pointing out that the choice of the specific instant herein considered is suggested only by the visual appearance of the grid and not by physical considerations. At the instant t_0 = 0.6 seconds the appearance of the grid results particularly effective and might help to understand the logic of the algorithm; for more details in this regard we refer to the work by Mazzei and Lettieri (10).

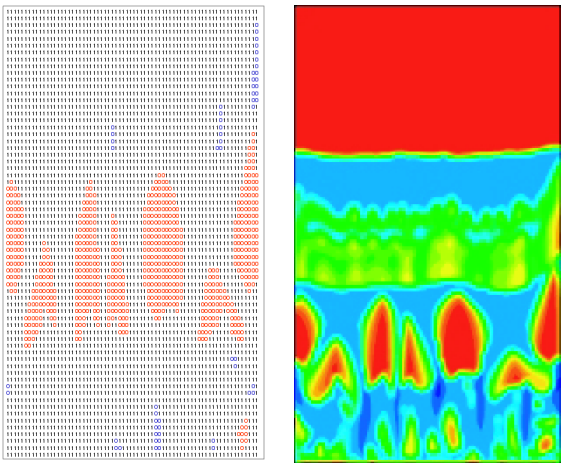

Figure 5a & 5b: Example of computational grid generated for the automatic calculation of the diameters of the bubbles featuring in the bed.

CONCLUSIONS

A multidimensional two-phase fluid dynamic model for fluidized beds has been briefly described and used to simulate the dynamics of liquid-solid and gas-solid fluidized powders belonging to Groups A and B of the Geldart's classification. The equations of motion have been solved using the commercial CFD code CFX 4.4. The investigation has been mainly concerned with the homogeneous and bubbling regimes of fluidization. The homogeneous bed computational study proposed to test computationally the validity of the drag force closure advanced by the authors. More than satisfactory results were found. The preliminary results of the computational study of the fluidization dynamics in bubbling beds have been reported. A numerical algorithm for the automatic computation of the bubbles diameters within the bed has been presented.

The 12th International Conference on Fluidization - New Horizons in Fluidization Engineering, Art. 84 [2007]

ACKNOWLEDGEMENTS

The authors wish to acknowledge financial support from the Engineering Physical Science Research Council (EPSRC) and BP Chemicals, Hull (UK), in particular Dr. Derek Colman.

REFERENCES

1. Geldart, D., “Types of fluidization”. Powder Technol. 7, 285-292 (1973).
2. Jackson, R., The dynamics of fluidized particles. Cambridge Monographs on Mechanics. Cambridge University Press, Cambridge (2000).
3. Bird, R.B., Stewart, W.E., Lightfoot, E.N., Transport Phenomena. Wiley, New York (2002).
4. Mazzei, L., Lettieri, P., Elson, T., Colman, D., “A revised mono-dimensional particle bed model for fluidized beds", Chem. Eng. Sci. 61, 1958-1972 (2006).
5. Happel, J., Epstein, N., “Viscous flow in multiparticle systems: cubical assemblages of uniform spheres", Ind. Eng. Chem. Vol. 46, 1187-1194 (1954).
6. Rumpf, H., Gupte, A.R., “Einflüsse der porosität und korngrößenverteilung im widerstandsgesetz der porenströmung", Chem. Ing. Tech. Vol. 43, 367–-375 (1971).
7. Wen, C.Y., Yu, Y.H., “Mechanics of Fluidization". Chem. Eng. Prog. Symp. Series 62, 100-111 (1966).
8. Ergun, S., “Fluid flow through packed columns". Chem. Eng. Progr. 48, 89-94 (1952).
9. Richardson, J.F., Zaki, W.N. “Sedimentation and Fluidization: Part I". Trans. Inst. Chem. Eng. 32, 35-53 (1954).
10. Mazzei, L., Lettieri, P., “A numerical algorithm for the analysis of the bubble dynamics in two-dimensional fluidized beds simulated by means of CFD codes", IJCRE, 4, A26, 1-18 (2006).